Fault Detection, Classification, and Location Based on Empirical Wavelet Transform-Teager Energy Operator and ANN for Hybrid Transmission Lines in VSC-HVDC Systems

Jalal Sahebkar Farkhani, Özgür Çelik, Kaiqi Ma, Claus Leth Bak, *Senior Member*, *IEEE*, and Zhe Chen, *Fellow*, *IEEE*

***Abstract*—Traditional protection methods are not suitable for hybrid (cable and overhead) transmission lines in voltage source converter based high-voltage direct current (VSC-HVDC) systems. Accordingly, this paper presents the robust fault detection, classification, and location based on the empirical wavelet transform-Teager energy operator (EWT-TEO) and artificial neural network (ANN) for hybrid transmission lines in VSC-HVDC systems. The operational scheme of the proposed protection method consists of two loops: ① an EWT-TEO based feature extraction loop, ② and an ANN-based fault detection, classification, and location loop. Under the proposed protection method, the voltage and current signals are decomposed into several sub-passbands with low and high frequencies using the empirical wavelet transform (EWT) method. The energy content extracted by the EWT is fed into the ANN for fault detection, classification, and location. Various fault cases, including the high-impedance fault (HIF) as well as noises, are performed to train the ANN with two hidden layers. The test system and signal decomposition are conducted by PSCAD/EMTDC and MATLAB, respectively. The performance of the proposed protection method is compared with that of the traditional non-pilot traveling wave (TW) based protection method. The results confirm the high accuracy of the proposed protection method for hybrid transmission lines in VSC-HVDC systems, where a mean percentage error of approximately 0.1% is achieved.**

***Index Terms*—Voltage source converter based high-voltage direct current (VSC-HVDC), protection, fault detection, fault classification, fault location, empirical wavelet transform (EWT), artificial neural network (ANN), hybrid transmission line.**

I. Introduction

THE transmission lines in the voltage source converter based high-voltage direct current (VSC-HVDC) systems have been extensively investigated, particularly for bulk power transmission over long distances with a high penetration of renewable energies [1]-[3]. In addition, the adoption of multi-terminal VSC-HVDC systems has been increasing because of the growing penetration of large-scale offshore wind farms into modern power networks [4]. Although the VSC-HVDC systems present several advantages over conventional high-voltage alternating current (HVAC) systems, ensuring the protection of VSC-HVDC systems remains a significant challenge in modern power systems [5].

Several protection methods for VSC-HVDC systems have previously been investigated. These methods are generally classified into traveling wave (TW) based protection method, differential protection method, derivative/transient based protection method, signal processing based protection method, and artificial intelligence (AI) based protection method. The TW-based protection method has been one of the main protection methods in power systems for many years. Although this method is applicable to both AC and DC systems, certain limitations warrant further investigation. These limitations include the variation in wave propagation velocities in hybrid (overhead and cable) transmission lines, potential susceptibility to noises, challenges in accurately detecting close-up faults, and a lack of mathematical tools for modeling [6], [7]. Consequently, the TW-based protection methods become more intricate when applied to hybrid transmission lines [7] and its effectiveness in accurate power system protection remains uncertain. The communication-based protection methods such as differential protection methods exhibit high accuracy and robustness against high-impedance faults (HIFs). Nevertheless, the communication-less (non-pilot) protection methods provide several advantages over communication-based protection methods, including high-speed performance, smaller measurement errors, enhanced cybersecurity, and the absence of communication costs [8], [9]. The derivative/transient based protection method relies on the rate of change of current and voltage. Although this method is primarily employed for fault detection, it encounters challenges in the accurate detection of HIFs in meshed high-voltage direct current (HVDC) systems [8]. Therefore, further research is required to overcome these limitations and enhance the protec-

Manuscript received: November 24, 2023; revised: April 8, 2024; accepted: September 3, 2024. Date of CrossCheck: September 3, 2024. Date of online publication: November 7, 2024.

J. S. Farkhani (corresponding author), K. Ma, C. L. Bak, and Z. Chen are with the Department of Energy, University of Aalborg, 9220 Aalborg, Denmark (e-mail: jsfa@energy.aau.dk; kma@energy.aau.dk; clb@energy.aau.dk; zch@energy.aau.dk).

Ö. Çelik is with Energy Systems Engineering Adana Alparslan Türkeş Science and Technology University, Adana, Turkey (e-mail: ozgurcelik@atu.edu.tr).

DOI: 10.35833/MPCE.2023.000925

tion performance in VSC-HVDC systems.

Recently, different signal processing methods and AI techniques have attracted considerable attention in power system protection. Several time-frequency signal processing methods, including the empirical mode decomposition (EMD), Hilbert-Huang transform (HHT), and wavelet transform (WT), have emerged as the most popular methods for signal feature extraction. These methods can effectively decompose the components of nonstationary and nonlinear signals. Although the EMD has been demonstrated to be effective in numerous applications, a significant limitation persists in the lack of theoretical analysis [10]. In addition, the HHT provides accurate and high-resolution outcomes but it still faces several challenges, such as a high computational burden, the absence of a stopping mode for the number of decomposition levels, and the sensitivity to noises [8]-[11]. The WT stands out as one of the most popular and widely utilized methods in time-frequency signal processing. However, it faces certain challenges, including a high computational burden and incomplete matching with all real signals. It is a complex task to select an appropriate mother WT type and decomposition level [12], [13]. The empirical wavelet transform (EWT) method has recently been proposed to address these challenges. It can determine the optimal number of filter banks, bandwidth, and central frequency for nonstationary signals [14]. The machine learning (ML) methods such as artificial neural networks (ANNs), support vector machines (SVMs), and decision trees (DTs) have been increasingly adopted in the field of protection. In [15], a fault detection and classification method based on the colony optimization and ANN for HVDC systems is developed, where WT is employed to extract signal features. This method enables the fault identification for two-terminal line commutated converters in HVDC transmission lines. In [16], a long short-term memory (LSTM) method for non-pilot protection of HVDC cable lines is presented. The signal data are extracted through the discrete wavelet transform (DWT).

Drawing on the findings of previous studies, the protection for hybrid transmission lines in VSC-HVDC systems remains a significant challenge. In this paper, a fault detection, classification, and location method is proposed based on the EWT-Teager energy operator (EWT-TEO) and ANN for hybrid transmission lines in VSC-HVDC systems. The performance of the proposed protection method is compared with that of a conventional non-pilot TW-based protection method using the same feature extraction process. Remarkably, the proposed protection method has a very high accuracy in fault location for hybrid transmission lines in VSC-HVDC systems. The main contributions of this paper are as follows.

1) This paper proposes a two-loop fault detection, classification, and location method for hybrid transmission lines in VSC-HVDC systems.

2) An adaptive time-frequency signal processing method, i. e., EMT, is employed to extract the signal features, and Teager energy operator (TEO) is used to capture the instantaneous amplitude and frequency changes of signals.

3) An optimized ANN using the signal features extracted by the EWT-TEO as its input parameters is proposed for accurate fault detection, classification, and location.

4) The proposed protection method is effective with a high fault resistance of 100 Ω and a noise of 20 dB.

5) The proposed protection method achieves a high accuracy and speed in comparison with the TW-based protection method and other existing methods.

The remainder of this paper is organized as follows. Section II briefly introduces the modular multilevel converter (MMC) in VSC-HVDC systems, particularly focusing on its behavior under DC short-circuit faults. Section III introduces the theory of the proposed protection method for the hybrid transmission lines in VSC-HVDC systems. Simulation results are presented and discussed in Section IV. Section V highlights the comparative results of the proposed protection method and the TW-based protection method. A conclusion is provided in Section VI.

II. Introduction of MMC

MMC typically has two types of submodules (SMs): the half-bridge (HB) SM and the full-bridge (FB) SM. The HB topology is commonly employed in commercial applications due to its inherent advantages. Figure 1 illustrates the structure of an MMC in VSC-HVDC system under a DC short-circuit fault. Each phase includes upper and lower arms, which consist of an N-series connection of SMs [17], [18]. In Fig. 1, FCL and DCCB are short for fault current limiter and DC circuit breaker, respectively.

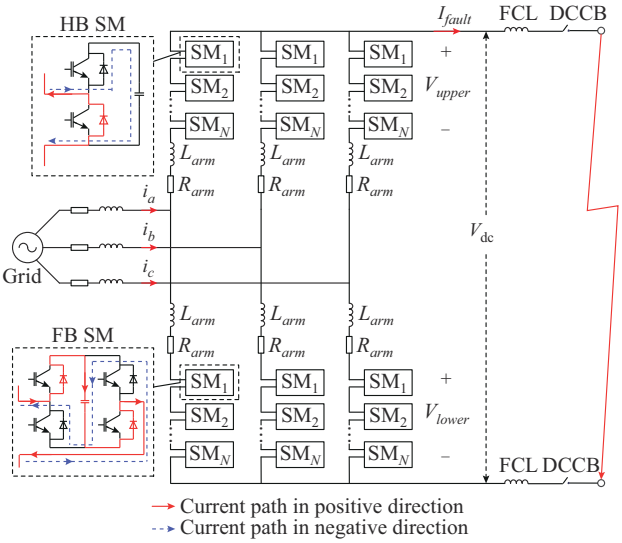

Fig. 1. Structure of MMC in VSC-HVDC system under a DC short-circuit fault.

The behavior of MMCs under a DC short-circuit fault can be divided into three different stages [18], [19]. At the initial stage, the MMC capacitors discharge immediately after the fault occurs [20]. Subsequently, the converter blocks through the parallel diode [21]. Finally, the short-circuit current is supplied from the AC grid. Since the fault should be detected very fast in VSC-HVDC systems, the proposed protection method utilizes data from the initial stage.

III. Theory of Proposed Protection Method

A. Data Processing

In this subsection, a dataset for training ML models is generated by applying various disturbances and faults to the VSC-HVDC system, which is modeled in PSCAD/EMTDC. Figure 2 outlines the operational mechanism of the proposed protection method, including the data-processing stages for training, where CB is short for circuit breaker; and CT and PT short for current transformer and potential transformer, respectively, which are used for measuring current and voltage signals.

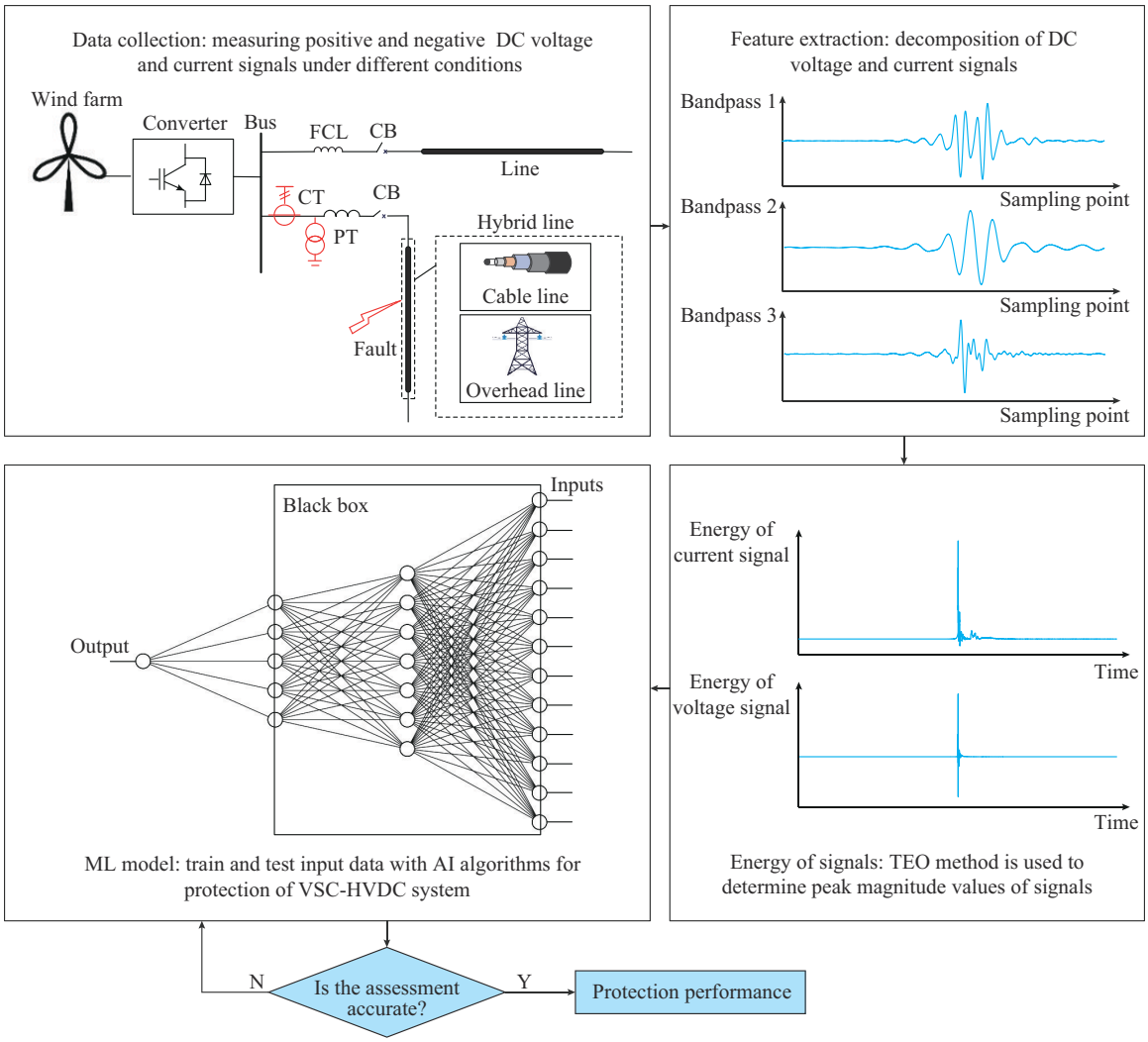

Fig. 2. Operational mechanism of proposed protection method.

1) Data collection: in real world, power grids may experience significant variations, encompassing various types of faults and disturbances [22]. Therefore, the data collection involves gathering information under different conditions, including non-fault, disturbance, and fault conditions. To validate the accuracy of the proposed protection method, the test system is simulated for various fault types, such as pole-to-pole (PtP), positive pole-to-ground (PtG), and negative pole-to-ground (NtG), at various distances between 2.5% and 97.5% of the transmission line. Different fault impedances ranging from 0.01 to 100 Ω and different signal-to-noise ratios (SNRs) ranging from 20 to 30 dB are also applied.

2) Feature extraction: EWT is an adaptive time-frequency signal processing method that decomposes signals into various modes based on their characteristics. It is used to select the most relevant features from the data and decompose them.

3) Energy of signals: the peak energy of each extracted signal is chosen as the input data for various AI algorithms. Once the data has been collected, they can be used to train the ML models.

B. EWT-TEO

The EWT [10] adaptively decomposes signals using the wavelet method. The main idea behind the EWT is to extract different signal features according to the Fourier segments and wavelet filter bank [23]. First, the Fourier transform is applied to the input signals, and then the segmentation of the Fourier spectrum is identified by locating the local maxima within the spectrum, which are sorted in decreasing order. The center between two adjacent local maxima is used to determine the boundaries of the Fourier segment.

This construction is similar to assembling a set of bandpass filters to decompose signals into distinct components [10]. In this method, the restriction $w \in [0,\pi]$ is considered along the Fourier axis to adhere to the Shannon criteria. The Fourier support $[0,\pi]$ is divided into N contiguous segments, and the boundaries w_n are determined between 0 and π. Each segment is represented as $\Lambda_n = [w_{n-1}, w_n]$, $n = 1, 2, \ldots, N$, and $\bigcup_{n=1}^{N} \Lambda_n = [0,\pi]$. Λ_n is defined by the EWT as a bandpass filter. Equations (1) and (2) represent the empirical scaling function $\hat{\Phi}_n(w)$ and empirical wavelet $\hat{\Psi}_n(w)$, respectively [10].

$$\hat{\Phi}_n(w) = \begin{cases} 1 & |w| \le (1-\gamma)w_n \\ \cos\left(\frac{\pi}{2}\beta\left(\frac{1}{2\gamma w_n}\left[|w| - 1(1-\gamma)w_n\right]\right)\right) & (1-\gamma)w_n \le |w| \le (1+\gamma)w_n \\ 0 & \text{otherwise} \end{cases} \tag{1}$$

$$\hat{\Psi}_n(w) = \begin{cases} 1 & (1+\gamma)w_n \le |w| \le (1-\gamma)w_{n+1} \\ \cos\left(\frac{\pi}{2}\beta\left(\frac{1}{2\gamma w_{n+1}}\left[|w| - 1(1-\gamma)w_{n+1}\right]\right)\right) & (1-\gamma)w_{n+1} \le |w| \le (1+\gamma)w_{n+1} \\ \sin\left(\frac{\pi}{2}\beta\left(\frac{1}{2\gamma w_n}\left[|w| - 1(1-\gamma)w_{n+1}\right]\right)\right) & (1-\gamma)w_n \le |w| \le (1+\gamma)w_n \\ 0 & \text{otherwise} \end{cases} \tag{2}$$

where γ is the coefficient; the transition function $\beta(x)$ is an arbitrary function, which can be expressed as:

$$\beta(x) = \begin{cases} 0 & x \le 0 \text{ or } \beta(x) + \beta(1-x) = 1, \forall x \in [0,1] \\ 1 & x \ge 1 \end{cases} \tag{3}$$

The most commonly used $\beta(x)$ is expressed as:

$$\beta(x) = x^4\left(35 - 84x + 70x^2 - 20x^3\right) \tag{4}$$

The coefficient γ $(0 < \gamma < 1)$ is defined as:

$$\gamma \prec \min\left(\frac{w_{n+1} - w_n}{w_{n+1} + w_n}\right) \tag{5}$$

The TEO is a nonlinear energy operator that can track and estimate the instantaneous energy of signals in the time domain. It is derived from the instantaneous amplitude and frequency variations of signals [24], [25]. Equation (6) expresses the continuous signals $x(t)$ using the TEO [26]:

$$\Psi\left(x(t)\right) = \dot{x}^2(t) - x(t)\ddot{x}(t) \tag{6}$$

where $\dot{x}$ and $\ddot{x}$ are the first-order derivative and second-order derivative of $x(t)$, respectively.

In the discrete domain, $x[n]$ is expressed as:

$$\Psi\left(x[n]\right) = \left(x[n]\right)^2 - x[n-1]x[n+1] \tag{7}$$

The energy of signals is then used to train the ML model for fault detection, classification, and location. The fault location error $Error_i$ and mean error M_{Error} are computed based on (8) and (9), respectively [27].

$$Error_i = \left|\frac{AFL_i - CFL_i}{l_t}\right| \tag{8}$$

$$M_{Error} = \frac{1}{M}\sum_{i=1}^{M} Error_i \tag{9}$$

where CFL_i and AFL_i are the calculated and actual fault distances, respectively; l_t is the total length of faulted line; and i and M are the index and number of samples, respectively.

C. ANN

In recent years, ML models have been widely applied in modeling nonlinear and complex systems, particularly in power systems. ANNs, inspired by AI, have been successful in data classification, pattern recognition, and prediction [28]. An ANN typically consists of several layers, including input, hidden, and output layers. Figure 3 shows the structure of an ANN with interconnected layers.

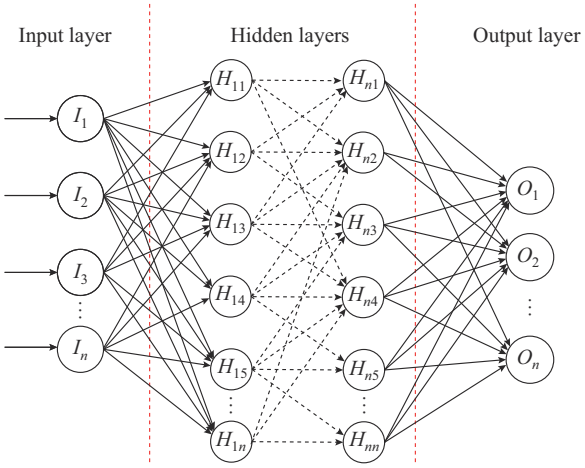

Fig. 3. Structure of ANN with interconnected layers.

The bilayer feedforward ANN consists of an input layer, two hidden layers with a set number of neurons, and an output layer. Despite the basic structure with only two hidden layers, a bilayer ANN offers advantages over single-layer perceptrons and paves the way for understanding architectures of deeper network. The optimal model can be achieved by evaluating various input combinations, such as the number of hidden layers, the number of neurons in hidden layers, and learning algorithms through different case studies. Increasing the number of hidden layers may enhance the accuracy of network prediction. Four types of learning algorithms, i.e., Levenberg-Marquardt, scaled conjugate gradient,

resilient backpropagation, and Polak-Ribiére conjugate gradient, have been previously tested and analyzed. Based on the test results, the Levenberg-Marquardt and scaled conjugate gradient learning algorithms are compared due to their superior accuracy. The input and target datasets are randomly divided into three subsets: training, testing, and validation datasets. The number of hidden neurons varies from 10 to 80 for evaluating the performance of the model with different numbers of hidden neurons.

The general neuron processing unit is given as:

$$\alpha = \phi\left(\sum_j \boldsymbol{w}_j \boldsymbol{x}_j + \boldsymbol{b}\right) \tag{10}$$

where α is the unit activation; $\boldsymbol{x}_j$ is the vector of unit inputs; $\boldsymbol{w}_j$ is the vector of weights; $\boldsymbol{b}$ is the vector of biases; and $\phi(\cdot)$ is the nonlinear activation function.

The first layer is the input layer, and its units correspond to the values of input features. The last layer is the output layer $\boldsymbol{y}_i$, which contains one unit for output value from each network. The layers between the input and output layers are known as hidden layers. The network unit receives connections from the units in the previous layer. This implies that each unit has its own bias and a weight w_{ij} exists for every pair of units in two consecutive layers. Consequently, the network computations can be expressed as [29]:

$$\begin{cases} \boldsymbol{h}_i^{(n)} = \phi^1\left(\sum_j w_{ij}^{(n)} \boldsymbol{x}_j + \boldsymbol{b}_i\right) \\ \boldsymbol{h}_i^{(n+1)} = \phi^2\left(\sum_j w_{ij}^{(n+1)} \boldsymbol{h}_i^{(n)} + \boldsymbol{b}_i^2\right) \\ \boldsymbol{y}_i = \phi^3\left(\sum_j w_{ij}^{(n+2)} \boldsymbol{h}_i^{(n+1)} + \boldsymbol{b}_i^3\right) \end{cases} \tag{11}$$

where $\boldsymbol{h}_i^{(n)}$ is the vector of units in the hidden layer; the subscript n is the index of hidden layer; and $\phi^1(\cdot)$, $\phi^2(\cdot)$, and $\phi^3(\cdot)$ are the distinct activation functions employed by different layers; and $\boldsymbol{b}_i$, $\boldsymbol{b}_i^2$, and $\boldsymbol{b}_i^3$ are the vectors of different biases.

D. TW Method

The principle of TW is based on the current and voltage waves propagating in both directions along the line after a fault occurs. This concept can be applied to both AC and DC lines, depending on the amplitude of the traveling wavefront. Figure 4 shows the TW propagation during a fault along the HVDC transmission line at the point with a distance of d from Bus M with incident and reflected waves. The total length of the fault line is l. The fault locator is positioned at Bus M.

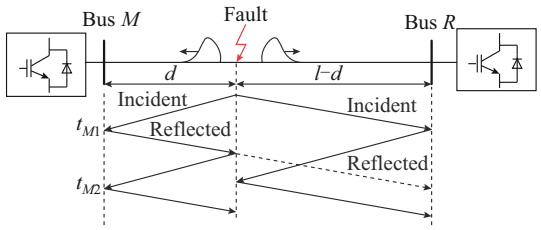

Fig. 4. TW propagation during a fault in HVDC transmission line.

The arrival time, denoted as t_{M1} and t_{M2}, corresponds to the first and second traveling wavefronts meeting at Bus M during the fault, respectively. The TW propagation velocity varies in the cable and overhead lines. The TW propagation velocity in overhead lines falls in the range of 290-299 m/μs, whereas in plastic and rubber cable lines, it exhibit approximately 170-200 and 210-230 m/μs, respectively. Therefore, the application of TW method to hybrid transmission lines is more complicated [7]. The wave propagation velocities of the aerial and ground modes are estimated to be approximately 295000 and 188000 km/s, respectively [30]. In this study, the wave propagation velocity is considered to be 181500 km/s. Equation (12) calculates d using the TW-based protection method.

$$d = \frac{v}{2}\left(t_{M2} - t_{M1}\right) \tag{12}$$

where v is the TW propagation velocity.

In addition, the TW-based protection method has other drawbacks, including the requirement of precise measurements of arrival time, challenges in mathematically modeling TWs, requirement of a high sampling rate, and susceptibility to noise interference.

In this study, an ANN with two hidden layers is utilized for fault detection, classification, and location for hybrid transmission lines in VSC-HVDC systems. Figure 5 presents a detailed flowchart of the proposed protection method for hybrid transmission lines in VSC-HVDC systems.

In the first step, the voltage and current signals are measured within a few milliseconds after a fault occurrence. These signals undergo feature extraction using the EWT, which decomposes the signal into different bandpass components. Then, the high-frequency features are extracted using the TEO. The EWT-TEO is utilized to extract suitable features, thereby enhancing the effectiveness of training the ML model. Finally, the ANN is employed to train the feature data for the purpose of achieving acceptable accuracy in the results. The model development process for the ANN will be explained in Section IV-C.

IV. Simulation Analysis

A. Test System

The test system consists of a four-terminal VSC-HVDC system utilizing the HB topology and control strategies modeled in PSCAD/EMTDC, as depicted in Fig. 6 [31]. Each HVDC converter of offshore wind plant (OWP) is connected to the load consumers, and line 1 connects two offshore HVDC converters. Table I presents the comprehensive parameters of the test system. The DCCB consists of a main CB and load branches that are connected in parallel. The DCCB operation details are explained in [32]. Different fault types, i.e., PtG, NtG, and PtP, are considered as different cases in this study. The test system includes two 100 km transmission lines (lines 1 and 3), a 200 km transmission line (line 2), and a 150 km transmission line (line 4). The candidate fault point is set on line 2, which is a hybrid line consisting of a 100 km overhead line and a 100 km cable line. The distance from the fault point to Bus 1 is denoted as d.

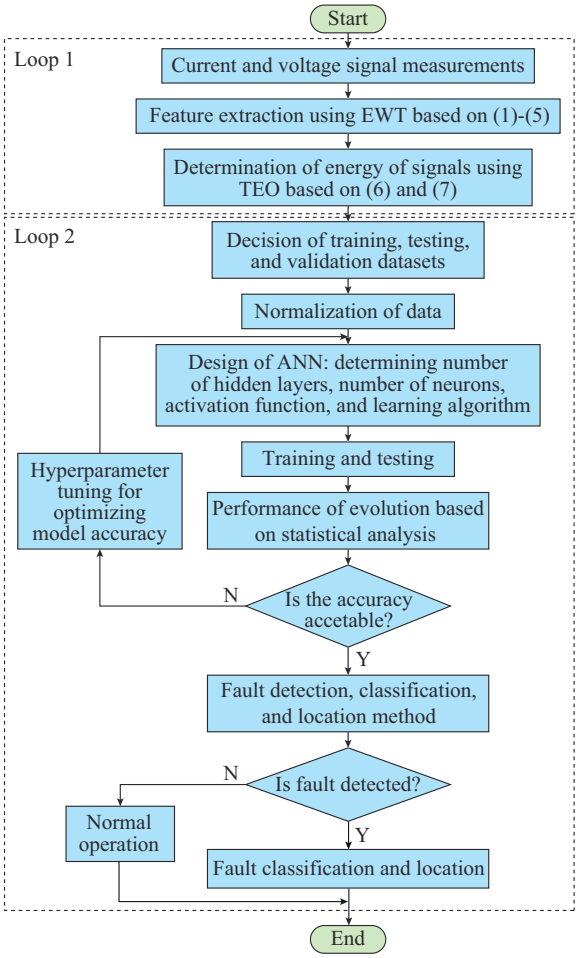

Fig. 5. Flowchart of proposed protection method.

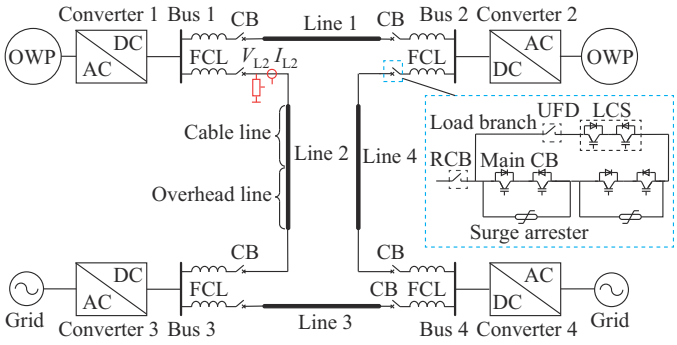

Fig. 6. Schematic of four-terminal VSC-HVDC system.

The current and voltage signal measurements in Fig. 6 are obtained from only one end of the transmission line using a single-ended protection method. In Fig. 6, UFD is short for ultra-fast disconnector, LCS is short for load commutation switch, and RCB is short for residual current breaker.

All faults occur at $t = 0.7$ s. The input data for ANN are measured approximately 1 ms after the fault occurs.

B. Data Preparation for Signal Decomposition

To validate the proposed protection method, different fault types with disturbances are simulated. Figure 7 shows the current signals under different fault types. As shown in Fig. 7(a), the two maximum fault currents differ by a factor of 7.

TABLE I
COMPREHENSIVE PARAMETERS OF TEST SYSTEM

Parameter	Value for converters 1-3	Value for converter 4
DC voltage (kV)	±320	±320
AC rated voltage (kV)	400	400
Sampling frequency (kHz)	20	20
AC converter voltage (kV)	380	380
Impedance (%)	15	15
Rated power (MW)	900	1200
Fault current limiter (mH)	100	100
Arm capacitance (μF)	29.3	39.0
Arm reactor L_{arm} (mH)	84.8	63.6
Arm resistance R_{arm} (Ω)	0.885	0.670
Bus filter reactor (mH)	10	10

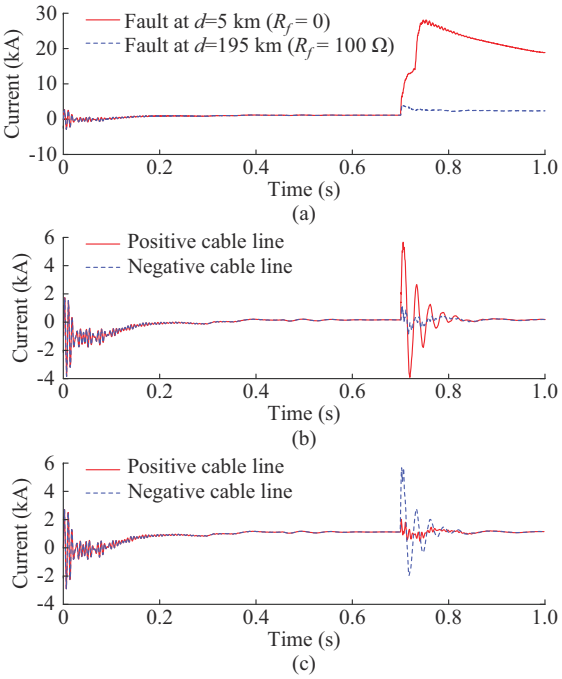

Fig. 7. Current signals under different fault types. (a) Solid PtP fault at d = 5 km and high impedance PtP fault at d = 195 km with an impedance of R_f = 100 Ω. (b) PtG fault at d = 20 km. (c) NtG fault at d = 180 km.

In this study, several passbands of EWT are used to decompose the current and voltage signals. These passbands enable the extraction of suitable data for analysis in this case study.

Figures 8 and 9 show the signal decomposition results using three passbands and one approximation coefficient of the EWT for current and voltage signals, respectively, under a PtP fault at d = 20 km. The EWT effectively decomposes the time-series signals into a set of passbands and an approximation coefficient.

Figure 10 shows the energy of the current and voltage signals after decomposition using Passband 1 as well as the trip signal under different fault types and distances when using the EWT.

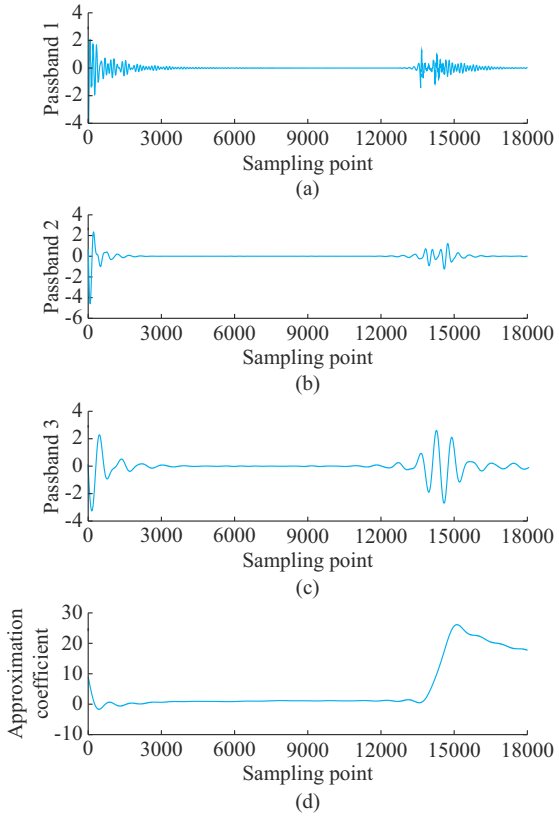

Fig. 8. Signal decomposition results using three passbands and one approximation coefficient of EWT for current signals under PtP fault. (a) Passband 1. (b) Passband 2. (c) Passband 3. (d) Approximation coefficient.

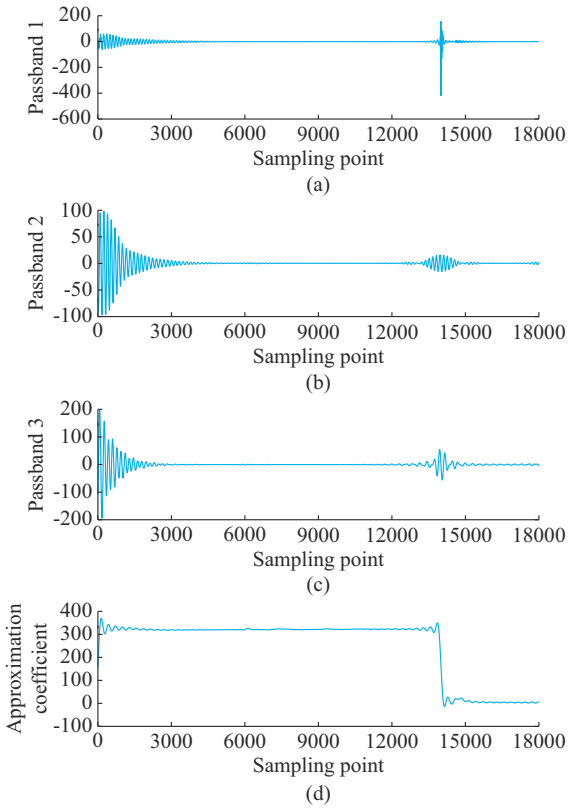

Fig. 9. Signal decomposition results using three passbands and one approximation coefficient of EWT for voltage signals under PtP fault. (a) Passband 1. (b) Passband 2. (c) Passband 3. (d) Approximation coefficient.

The protection time required includes signal processing, ANN computation, and protection relay tripping. The fault detection time t_d for current and voltage signals is measured at 0.70005 s, which is 0.05 ms after the fault occurrence, as shown in Fig. 10(a). Consequently, the fault detection time is exceptionally short under the proposed protection method. The moving windowing technique employed in the EWT enables the online monitoring and facilitates fault detection within partial segments without considering the entire window. The maximum data window length utilized in this study is less than 0.25 ms. The training time for ANN is approximately 22 min, and the protection time of the developed model aligns with the simulation solution time step, which is set to be 100 μs. A measurement time delay can also be added to the protection time, which is estimated to be approximately 0.1 ms. The tripping signal time t_s represents the protection time, which includes both computational time and delay, which are both 1 ms in this study. As shown in Fig. 10(b), t_d and t_s are approximately 0.7001 and 0.7011 s, respectively, which is 0.1 and 1.1 ms after the fault occurrence. The peak time of signals is 0.70015 s, which is 0.15 ms after the fault occurrence.

C. Data Preparation and Training

The proposed protection method is trained in several non-fault and fault states with different fault types, distances, fault resistances, noises, and line outages, to obtain a dataset that encompasses all possible operating conditions. The EWT is applied to extract the signal features. Indeed, the suitable extracted features from the original data lead to better training. Table II lists parameters of simulated non-fault and fault states for the training dataset.

The input data matrix of ANN is created using different case studies of the VSC-HVDC system for fault detection, location, and classification. Several fault locations and fault types are considered during the dataset preparation. In addition, several fault resistances and high-level noises are included to enhance the sensitivity and selectivity of the developed model. The input data matrix ***Maxb*** includes 464 rows that illustrate the number of conducted cases and 16 columns that show the number of voltage/current features extracted in each case study. The output data matrix ***Naxb*** has 464 rows that represent the target values and 7 columns that represent the fault detection, fault location, fault types, fault resistance, and noise.

Each column of the created input and output data matrices is individually normalized to scale the values within a specific range. The resulting dataset is randomly divided into three subsets: training, validation, and testing datasets. The numbers of neurons in the hidden layers are chosen as 40 and 50 following several attempts based on the optimal error analysis. The main objectives at this stage are to achieve high accuracy with the desired mean squared error and prevent overfitting to obtain a more general model. The input activation function is a hyperbolic tangent sigmoid function, and the output activation function is a linear activation function. Following tests of several learning algorithms, we find that the best results are obtained with the Levenberg-Marquardt learning algorithm.

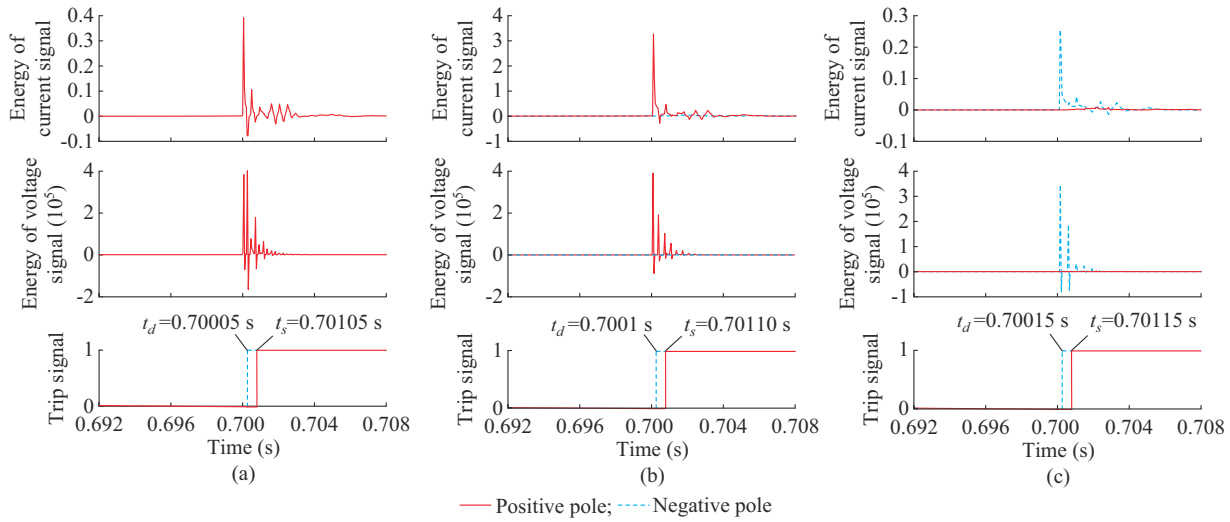

Fig. 10. Energy of current and voltage signals after decomposition as well as trip signal using Passband 1 under different fault types and distances. (a) Under PtP fault at $d=20$ km. (b) Under PtG fault at $d=30$ km. (c) Under NtG fault at $d=40$ km.

TABLE II
PARAMETERS OF SIMULATED NON-FAULT AND FAULT STATES

State	Description	Parameter
Fault state	Fault type	PtP, NtG, and PtG
	d (km)	[5, 195]
	R_f (Ω)	0.01, 10, 50, and 100
	SNR (dB)	[20, 30]
Non-fault state	Outage lines	Line 1, line 3, and line 4

At the training stage, the system parameters are adjusted as follows. The minimum performance gradient is 10^{-8}, the maximum number of epochs is 1000, and the maximum validation failure is 50. Due to the random assignment of weights and bias values, the model is retrained for 50 times to identify the model with the best performance. Figure 11 shows the regression analysis of the trained neural network with the proposed protection method. The training dataset and the effect of noises on the training process are analyzed, as shown in Fig. 11(b).

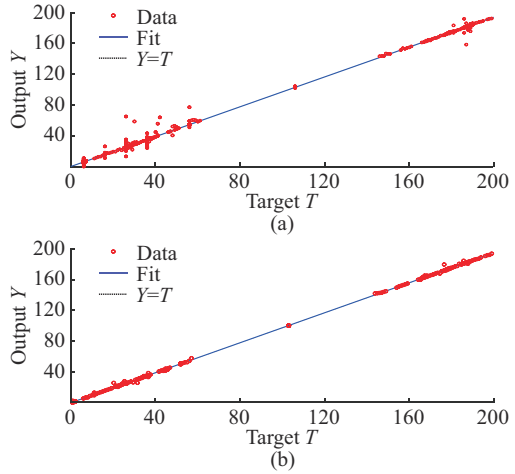

Fig. 11. Regression analysis of trained neural network for proposed protection method. (a) Under HIF with noises ($Y=T+0.079$). (b) Under HIF without noises ($Y=T+0.039$).

The regression for the dataset improves by approximately 0.09% without noises. Noises at random frequencies and fault impedances are considered during the dataset preparation to increase the sensitivity and selectivity of the proposed protection method. However, the noises can introduce variability and inaccuracies in the training process, leading to suboptimal performance. To address these issues, the training dataset is adjusted to incorporate several cases. Data cleaning and augmentation methods are utilized to deal with the effects of noise on the training of ANN. At the data cleaning stage, the noisy data points are filtered out from the training datasets prior to model training. At the data augmentation stage, the existing datasets are enhanced to increase their diversity and reduce the effects of noises. Finally, the ANN is trained using different subsets of data to reduce the effects of noise and enhance generalization.

D. ANN Testing

The ANN is tested using a separate dataset that is not utilized at the training stage. This dataset includes different fault types, locations, resistances, and high-level noises.

Table III presents the results obtained for the fault detection, classification, and location with the proposed protection method. The training process consists of three sections: fault detection, classification, and location. The results for the non-fault states are also presented in Table III. The proposed protection method can diagnose non-fault and fault modes. The output of the ML model is classified into different fault types. For example, an NtG fault corresponds to the classifier outputs [0 1 1], whereas the PtN fault is represented by the classifier outputs [1 1 0]. As a result, the mean absolute error of the proposed protection method is approximately 0.167%.

Table IV presents the fault location results with different fault resistances and noises. As mentioned above, the accuracy of ANN decreases in the presence of noises. Therefore, different SNRs along with varying fault resistances are considered to create a robust and accurate model.

TABLE III
FAULT DETECTION, IDENTIFICATION, AND LOCATION WITH PROPOSED PROTECTION METHOD

d (km) or outage line	Fault type	Classifier output	Is fault detected?	Calculated distance (km)	Error (%)
6.0	PtN	[1 1 0]	Yes	5.9625	0.0187
8.5	PtN	[1 1 0]	Yes	9.0242	0.2621
16.0	PtN	[1 1 0]	Yes	15.8959	0.0525
28.5	PtN	[1 1 0]	Yes	27.8617	0.3195
30.0	PtN	[1 1 0]	Yes	30.3546	0.1770
33.0	PtG	[1 0 1]	Yes	32.8708	0.0650
40.0	NtG	[0 1 1]	Yes	40.1482	0.0740
41.0	PtG	[1 0 1]	Yes	41.0118	0.0055
44.0	NtG	[0 1 1]	Yes	44.0076	0.0083
55.0	NtG	[0 1 1]	Yes	56.6316	0.8155
145.0	PtG	[1 0 1]	Yes	145.0445	0.0222
155.0	PtG	[1 0 1]	Yes	154.9132	0.0450
160.0	NtG	[0 1 1]	Yes	160.8540	0.4270
162.0	PtN	[1 1 0]	Yes	162.6980	0.3450
162.3	PtN	[1 1 0]	Yes	161.8509	0.2250
174.0	NtG	[0 1 1]	Yes	173.9353	0.0325
176.0	PtN	[1 1 0]	Yes	175.4677	0.2660
189.0	PtN	[1 1 0]	Yes	189.1934	0.0965
191.5	PtN	[1 1 0]	Yes	191.5763	0.0380
194.0	PtN	[1 1 0]	Yes	193.9071	0.0465
Line 1			No		
Line 4			No		

V. PERFORMANCE ANALYSIS

Table V compares the fault location results using the TW-based protection method with different sampling frequencies and the proposed protection method. As can be observed, the accuracy of the proposed protection method is higher than that of the TW-based protection method. The sampling frequency affects the accuracy of the TW-based protection method. Higher sampling frequencies lead to reduced fault location errors. However, the fact that using a higher sampling frequency also results in a higher computational burden. In addition, the TW-based protection method has drawbacks such as increased complexity when dealing with hybrid transmission lines. Due to the different propagation velocities of the cable and overhead lines, the accuracy of the TW-based protection method is inadequate for both line sections. Figure 12 shows the fault location results using the TW-based protection method at different fault distances, employing the current signal. As Fig. 12 shows, the error in the fault location increases on the overhead line due to different propagation velocities.

TABLE IV
FAULT LOCATION RESULTS WITH DIFFERENT FAULT RESISTANCES AND NOISES

SNR (dB)	*d* (km)	Calculated distance with different fault resistances (km)		
		0.01 Ω	10 Ω	100 Ω
0	22	21.43510	22.4770	20.7638
	24	23.93590	23.0754	24.4008
	181	180.61410	180.6404	181.5918
	183	182.58740	182.9955	182.6885
	184	184.02590	184.1146	183.8375
20	21	20.67510	20.8616	22.0671
	22	21.64930	21.8189	23.0442
	23	21.77100	22.7092	22.8557
	181	180.86890	180.9329	181.6130
	184	184.00478	183.9893	184.8035
30	21	21.11510	21.1975	20.2647
	22	22.24350	22.0053	21.7527
	181	181.10360	180.8938	181.4932
	182	182.01090	182.1036	182.5961
	184	183.91570	184.1752	184.7559

TABLE V
COMPARISION OF FAULT LOCATION RESULTS WITH DIFFERENT METHODS FOR HYBRID TRANSMISSION LINE

Line	*d* (km)	Fault type	Classifier output	Error (%)			
				TW-based protection method with different sampling frequencies			Proposed protection method
				20 kHz	100 kHz	200 kHz	
Cable	6.0	PtN	[1 1 0]	0.73120	0.27750	0.05060	0.0187
	8.5	PtN	[1 1 0]	0.28750	0.28750	0.16700	0.2621
	16.0	PtN	[1 1 0]	1.19370	0.16750	0.05930	0.0525
	30.0	PtN	[1 1 0]	0.88120	0.42750	0.42750	0.1770
	41.0	PtG	[1 0 1]	0.08125	0.08125	0.16250	0.0055
	55.0	NtG	[0 1 1]	0.27500	0.17875	0.04812	0.8155
Overhead	145.0	PtG	[1 0 1]	2.16870	1.71500	1.03430	0.0222
	160.0	NtG	[0 1 1]	1.67500	1.22000	0.59300	0.4270
	176.0	PtN	[1 1 0]	5.01750	5.00000	4.11100	0.2660
	189.0	PtN	[1 1 0]	8.28750	6.23000	4.87100	0.0965
	194.0	PtN	[1 1 0]	High	10.99000	7.36500	0.0465

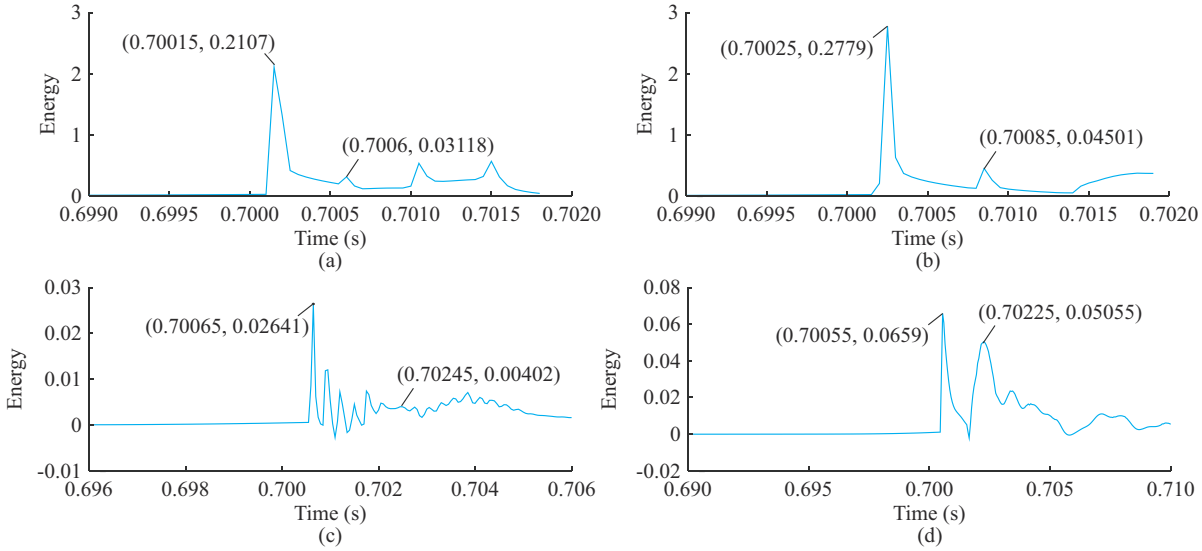

Fig. 12. Fault location results of TW-based protection method at different distances. (a) $d = 41$ km (cable line). (b) $d = 55$ km (cable line). (c) $d = 160$ km (overhead line). (d) $d = 194$ km (overhead line).

Table VI presents a comparative assessment of the proposed protection method with other protection methods in the recent literature for hybrid transmission lines in VSC-HVDC systems. As can be observed, the proposed protection method has a higher accuracy, which can also detect and classify different fault types. Moreover, the proposed protection method does not require high sampling frequency and communication links.

TABLE VI
COMPARATIVE ASSESSMENT OF PROPOSED PROTECTION METHOD WITH OTHER PROTECTION METHODS

Reference	Year	Method	Which signal is used?	Sampling frequency (kHz)	Fault classification	Fault location	Is communication required?	Is noise existed?	The maximum fault resistance (Ω)	Mean fault location error (%)
[3]	2023	DWT	Voltage	100	+	+	No	Yes	500	0.33
[4]	2023	ANN	Voltage	2.5	–	+	No	No	100	0.53
[33]	2022	ANN	Voltage	10-20	–	+	No	No	500	0.64
[34]	2021	SSA	Voltage	250	+	+	No	Yes	450	0.50
[35]	2019	Wavelet	Current	50-200	–	+	Yes	No	300	0.44
[36]	2018	SAE	Current	5000	–	+	No	Yes	100	0.71
[37]	2015	EEMD	Voltage	1000	–	+	Yes	No	100	1.00
[38]	2013	Distance/ FDPM	Both voltage and current	80	–	+	No	No	100	3.60
[39]	2009	DPLM	Both voltage and current	100	+	+	Yes	No	500	0.32
Proposed		EWT-ANN	Both voltage and current	20	+	+	No	Yes	100	0.10

Note: SSA is short for signal segmentation approach, SAE is short foe Stacked auto-encode, EEMD is short for ensemble empirical mode decomposition, FDPM is short for frequency-dependent parameter model, and DPLM is short for distributed parameter line model. The symbol + indicates that the fault classification or location method is included in the corresponding reference, and the symbol – indicates that the fault classification or location method is not included in the corresponding reference.

VI. CONCLUSION

Conventional protection methods are not applicable to the hybrid transmission lines in VSC-HVDC systems. This paper presents the fault detection, classification, and location method based on the EWT-TEO and ANN. The EWT is employed for feature extraction from the voltage and current signals. The TEO is then applied to compute the instantaneous energy of the processed signals. Finally, an ANN is utilized for fault detection, location, and classification under various case studies. The results show that the proposed protection method is a robust candidate due to its high accuracy and rapid performance in fault detection, classification, and location. The proposed protection method outperforms the existing methods including the TW-based protection method. The proposed protection method exhibits a high accuracy of greater than 99.90%, even in the presence of high levels of

noises and HIFs and achieves a fault detection time of approximately 1 ms. In general, the proposed protection method offers high-speed performances in fault detection and classification. The performance of the proposed protection method is analyzed under different simulation scenarios in the test system. The robustness of the proposed protection method across various fault resistances and high-level noises is validated.

REFERENCES

[1] A. Imani, Z. Moravej, and M. Pazoki, "A novel MODWT-based fault detection and classification scheme in VSC-HVDC transmission line," *Electric Power Systems Research*, vol. 221, p. 109434, Aug. 2023.

[2] P. Xing, Y. Yang, J. Peng *et al*., "Analysis of VSC-HVDC support capability for power grids with large-scale renewable energy and multi-infeed HVDC links," *Energy Reports*, vol. 9, pp. 1084-1091, Sept. 2023.

[3] M. Fayazi, M. Joorabian, A. Saffarian *et al*., "A single-ended traveling wave based fault location method using DWT in hybrid parallel HVAC/HVDC overhead transmission lines on the same tower," *Electric Power Systems Research*, vol. 220, p. 109302, Jul. 2023.

[4] S. H. A. Niaki, J. S. Farkhani, Z. Chen *et al*., "An intelligent method for fault location estimation in HVDC cable systems connected to offshore wind farms," *Wind*, vol. 3, no. 3, pp. 361-374, Aug. 2023.

[5] A. Pragati, M. Mishra, P. K. Rout *et al*., "A comprehensive survey of HVDC protection system: fault analysis, methodology, issues, challenges, and future perspective," *Energies*, vol. 16, no. 11, p. 4413, May 2023.

[6] Q. Yang, S. L. Blond, R. Aggarwal *et al*., "New ANN method for multi-terminal HVDC protection relaying," *Electric Power Systems Research*, vol. 148, pp. 192-201, Jul. 2017.

[7] F. Deng, X. Zeng, X. Tang *et al*., "Travelling-wave-based fault location algorithm for hybrid transmission lines using three-dimensional absolute grey incidence degree," *International Journal of Electrical Power & Energy Systems*, vol. 114, p. 105306, Jan. 2020.

[8] J. S. Farkhani, Ö. Çelik, K. Ma *et al*., "A comprehensive review of potential protection methods for VSC multi-terminal HVDC systems," *Renewable and Sustainable Energy Reviews*, vol. 192, p. 114280, Mar. 2024.

[9] B. Li, J. He, Y. Li *et al*., "A review of the protection for the multi-terminal VSC-HVDC grid," *Protection and Control of Modern Power Systems*, vol. 4, no. 3, pp. 1-11, Jul. 2019.

[10] J. Gilles, "Empirical wavelet transform," *IEEE Transactions on Signal Processing*, vol. 61, no. 16, pp. 3999-4010, Aug. 2013.

[11] S. Javaid, D. Li, and A. Ukil, "Transient analysis method using high pass filter circuit in VSC interfaced multi-terminal DC system," *Electric Power Systems Research*, vol. 216, p. 109062, Mar. 2023.

[12] W. Liu and W. Chen, "Recent advancements in empirical wavelet transform and its applications," *IEEE Access*, vol. 7, pp. 103770-103780, Jul. 2019.

[13] G. N. Lopes, T. S. Menezes, G. G. Santos *et al*., "High Impedance Fault detection based on harmonic energy variation via S-transform," *International Journal of Electrical Power & Energy Systems*, vol. 136, p. 107681, Mar. 2022.

[14] H. A. Mohammadi, S. Ghofrani, and A. Nikseresht, "Using empirical wavelet transform and high-order fuzzy cognitive maps for time series forecasting," *Applied Soft Computing*, vol. 135, p. 109990, Mar. 2023.

[15] R. S. Jawad and H. Abid, "HVDC fault detection and classification with artificial neural network based on ACO-DWT method," *Energies*, vol. 16, no. 3, p. 1064, Jan. 2023.

[16] M. Z. Yousaf, H. Liu, A. Raza *et al*., "Deep learning-based robust DC fault protection scheme for meshed HVDC grids," *CSEE Journal of Power and Energy Systems*, vol. 9, no. 6, pp. 2423-2434, Nov. 2023.

[17] H. Xiao, H. Gan, P. Yang *et al*., "Robust submodule fault management in modular multilevel converters with nearest level modulation for uninterrupted power transmission," *IEEE Transactions on Power Delivery*, vol. 39, no. 2, pp. 931-946, Apr. 2024.

[18] H. Li, Q. Wang, Q. Wu *et al*., "Capacitor voltage balancing method for hybrid modular multilevel converters based on second-harmonic voltage injection," *Journal of Power Electronics*, vol. 24, no. 4, pp. 553-564, Jan. 2024.

[19] C. Hou, X. Zhang, Z. Ye *et al*., "A new method for analyzing the permanent short- circuit fault characteristics of MMC converter," in *Proceedings of 2021 8th International Forum on Electrical Engineering and Automation* (*IFEEA*), Xi'an, China, Sept. 2021, pp. 128-132.

[20] N. Liu, Y. Li, X. Chen *et al*., "A novel protection based on current correlation for DC lines in hybrid cascaded multi-terminal HVDC transmission system," *IEEE Transactions on Power Delivery*, vol. 38, no. 4, pp. 2794-2809, Aug. 2023.

[21] R. H. Chandio, F. A. Chachar, J. B. Soomro *et al*., "Control and protection of MMC-based HVDC systems: a review," *Energy Reports*, vol. 9, pp. 1571-1588, Dec. 2023.

[22] H. Xiao, H. He, L. Zhang *et al*., "Adaptive grid-synchronization based grid-forming control for voltage source converters," *IEEE Transactions on Power Systems*, vol. 39, no. 2, pp. 4763-4766, Mar. 2024.

[23] Y. M. Hsueh, V. R. Ittangihal, W. Wu *et al*., "Fault diagnosis system for induction motors by CNN using empirical wavelet transform," *Symmetry*, vol. 11, no. 10, p. 1212, Sept. 2019.

[24] Z. Wang, J. Yang, H. Li *et al*., "Improved cyclostationary analysis method based on TKEO and its application on the faults diagnosis of induction motors," *ISA Transactions*, vol. 128, no. A, pp. 513-530, Sept. 2022.

[25] L. Kerkeni, Y. Serrestou, K. Raoof *et al*., "Automatic speech emotion recognition using an optimal combination of features based on EMD-TKEO," *Speech Communication*, vol. 114, pp. 22-35, Nov. 2019.

[26] E. Kvedalen, "Signal processing using the Teager energy operator and other nonlinear operators," *Master's Thesis, University of Oslo*, Oslo, Norway, May 2003.

[27] B. Shang, G. Luo, M. Li *et al*., "Transfer learning-based fault location with small datasets in VSC-HVDC," *International Journal of Electrical Power & Energy Systems*, vol. 151, p. 109131, Sept. 2023.

[28] A. Moradzadeh, A. Mansour-Saatloo, M. Nazari-Heris *et al*., *Wind Speed Forecasting Using Innovative Regression Applications of Machine Learning Techniques*. Cham: Springer International Publishing, 2021.

[29] A. Kurani, P. Doshi, A. Vakharia *et al*., "A comprehensive comparative study of artificial neural network (ANN) and support vector machines (SVM) on stock forecasting," *Annals of Data Science*, vol. 10, no. 1, pp. 183-208, Jan. 2023.

[30] G. Krzysztof, R. Kowalik, D. Rasolomampionona *et al*., "Traveling wave fault location in power transmission systems: an overview," *Journal of Electrical Systems*, vol. 7, no. 3, pp. 287-296, Sept. 2011.

[31] W. Leterme, N. Ahmed, J. Beerten *et al*., "A new HVDC grid test system for HVDC grid dynamics and protection studies in EMT-type software," in *Proceedings of 11th IET International Conference on AC and DC Power Transmission*, Birmingham, UK, Feb. 2015, pp. 1-7.

[32] M. Callavik, A. Blomberg, J. Häfner *et al*., "The hybrid HVDC breaker," *ABB Grid Systems Technical Paper*, vol. 361, pp. 143-152, Nov. 2012.

[33] M. M. Elgamasy, M. A. Izzularab, and X. P. Zhang, "Single-end based fault location method for VSC-HVDC transmission systems," *IEEE Access*, vol. 10, pp. 43129-43142, Apr. 2022.

[34] M. Farshad and M. Karimi, "A signal segmentation approach to identify incident/reflected traveling waves for fault location in half-bridge MMC-HVDC grids," *IEEE Transactions on Instrumentation and Measurement*, vol. 71, p. 3501209, Dec. 2022.

[35] X. Zhang, N. Tai, X. Zheng *et al*., "Wavelet-based EMTR method for fault location of VSC-HVDC transmission lines," *The Journal of Engineering*, vol. 2019, no. 16, pp. 961-966, Mar. 2019.

[36] G. Luo, C. Yao, Y. Liu *et al*., "Stacked auto-encoder based fault location in VSC-HVDC," *IEEE Access*, vol. 6, pp. 33216-33224, Jun. 2018.

[37] J. Liu, J. Duan, H. Lu *et al*., "Fault location method based on EEMD and traveling-wave speed characteristics for HVDC transmission lines," *Journal of Power and Energy Engineering*, vol. 3, no. 4, pp. 106-113, Apr. 2015.

[38] J. Suonan, J. Zhang, Z. Jiao *et al*., "Distance protection for HVDC transmission lines considering frequency-dependent parameters," *IEEE Transactions on Power Delivery*, vol. 28, no. 2, pp. 723-732, Apr. 2013.

[39] J. Suonan, S. Gao, G. Song *et al*., "A novel fault-location method for HVDC transmission lines," *IEEE Transactions on Power Delivery*, vol. 25, no. 2, pp. 1203-1209, Apr. 2010.

Jalal Sahebkar Farkhani received the M.Sc. degree in electrical engineering from Birjand University, Birjand, Iran, in 2012. Since 2021, he has been a Ph.D. student at the Department of Energy, Aalborg University, Aalborg, Denmark. His research interests include power system protection, voltage source converter based high-voltage direct current (VSC-HVDC) system,

distributed generation, and dynamic of wind turbine.

Özgür Çelik received the M.Sc. and Ph.D. degrees from the Department of Electrical and Electronics Engineering, Çukurova University, Adana, Turkey, in 2015 and 2019, respectively. His research interests include control of power electronic converter, grid integration of renewable energy system, and energy efficiency application.

Kaiqi Ma received the B.Eng. and M.Eng. degrees in control engineering from Hohai University, Nanjing, China, in 2012 and 2015, respectively. He was Research Associate at Research & Development Center of State Grid Xuji Group Corporation, Xuchang, China. Since 2018, he has been a Ph.D. student at the Department of Energy, Aalborg University, Aalborg, Denmark. His research interests include distributed generation, advanced control, and power system protection.

Claus Leth Bak received the B.Sc. and M.Sc. degrees in electrical power engineering from the Department of Energy Technology, Aalborg University, Aalborg, Denmark, in 1992 and 1994, respectively, and the Ph.D. degree with the thesis "EHV/HV underground cables in the transmission system" from Aalborg University, in 2015. He is a Full Professor with the Department of Energy Technology, Aalborg University. His Research interests include corona phenomena on overhead line, composite transmission tower, power system modeling and transient simulation, underground cable transmission, power system harmonics, power system protection, composite materials for extra high-voltage (EHV) power pylon, and VSC-HVDC offshore transmission network.

Zhe Chen received the B.Eng. and M.Sc. degrees in electrical engineering from Northeast China Institute of Electric Power Engineering, Jilin, China, and the Ph.D. degree in power and control from the University of Durham, Durham, U.K., in 1997. He is a Full Professor with the Department of Energy Technology, Aalborg University, Aalborg, Denmark. He is the Leader of the Wind Power System Research Program with the Department of Energy Technology, Aalborg University, and the Danish Principal Investigator for the Wind Energy of Sino-Danish Centre for Education and Research. His research interests include power system, power electronics, electric machine, wind energy, and modern power system.